

# Modelling and Analysis of Salient-Pole Rotor Interior Permanent Magnet Synchronous Motor for Oil and Gas Pump Applications

Ayebatonye Marttyns Epemu\* and Donatus Uchechukwu Onyishi  
*Department of Electrical/Electronic Engineering, Federal University of Petroleum Resources, Effurun, Nigeria.*

## Abstract

*This paper presents the design and dynamic simulation of a line-start, three-phase Interior Permanent Magnet Synchronous Motor (IPMSM) intended for pump applications in the oil and gas industry. The problem addressed in this paper pertains to the replacement of an existing induction motor (IM) in an oil and gas pump station with a more efficient and controllable solution, the IPMSM since IMs are known to be less efficient and IPMSM is easier to control. The chosen motor type employs a traditional salient-pole rotor with cage windings, known for its line-start capability, making it a feasible choice for constant-speed and pump applications. The dynamic simulation of the proposed IPMSM is carried out using MATLAB/Simulink, focusing on fundamental harmonic analysis in direct-phase variables. The results demonstrate rapid startup to synchronous speed with minor deviations effectively dampened by the rotor's damper windings. Torque characteristics exhibit some pulsations caused by magneto-motive force (MMF) harmonics; a phenomenon captured by Finite Element Analysis (FEA). The performance results show that the proposed IPMSM with a salient-pole rotor is viable and a promising replacement for induction motors in oil and gas pump stations.*

**Keywords:** *Mathematical modelling, Dynamic simulation, Direct-phase variables, Finite Element Analysis, Interior permanent magnet motor.*

## 1. Introduction

The criteria are stringent, and the capacity of centrifugal submersible pumps increases as a result of the expansion of oil production from wells under challenging conditions, such as deep drilling, high reservoir fluid temperatures, etc. The design and implementation of a permanent magnet-assisted synchronous reluctance motor for pump application were presented in [1]. Also, the development of submersible pumps using permanent magnet motors, designed for the oil and gas industry was presented in [2]. The main reason for the choice of permanent magnet motors is because of their high power density, high power factor, high efficiency, and ability to work under high temperatures [3], [4]. Recently, several improvements have been made to the IPMSM; examples of such improvements are the use of multiple phases for fault-tolerant purposes and torque improvements [5], the use of dual-stator windings for power factor improvement [6], and rotor optimization [7], [8].

There are several methods of modelling electrical machines, such as the D-Q method [9], the magnetic equivalent circuit method [10], the direct-phase variable method [11]–[13], and also the use

---

\* Corresponding author.

E-mail address: epemu.ayebatonye@fupre.edu.ng

Manuscript History:

Received 23 October, 2022, Revised 2 October, 2023, Accepted 2 October, 2023, Published 31 October, 2023

Copyright © 2023 UNIMAS Publisher. This is an open access article under the CC BY-NC-SA 4.0 license.

<https://doi.org/10.33736/jaspe.5087.2023>

of Finite Element Analysis (FEA) [14]. The method used in this study is the direct-phase variable method. The choice of this method is mainly because it avoids the use of complex mathematical transformations that are involved in the conventional D-Q method. Another advantage of this method over the D-Q is that spatial harmonics and saturation can be directly included in the mathematical modelling. Although the FEA method requires more machine information and takes a long time to simulate, it is deemed the most accurate as the results are close to the actual behaviour of the machine in real life.

The rotors of IPMSM are mainly cylindrical rotors with permanent magnet bars inserted inside. Surface permanent magnet synchronous can be cylindrical or salient [6], [15]. The use of permanent magnets in improving rotor saliency of synchronous reluctance motors having axially and transversely laminated rotors is well known [16]. The salient pole rotor with cage windings was used in this study as opposed to complex rotor types such as the axially laminated rotor and the transversely laminated rotor, which are more difficult to model and manufacture with respect to their complex rotor design with flux barriers. The mathematical modelling of the salient pole rotor used in the study is similar to what was presented in [17].

The growing demands of centrifugal submersible pumps, driven by the expansion of oil production under challenging conditions, such as deep drilling and high reservoir fluid temperatures, require efficient and robust motor solutions. The paper presents the design and dynamic simulation of a proposed line-start, three-phase Interior Permanent Magnet Synchronous Motor (IPMSM) intended for pump applications in the oil and gas industry. The chosen motor type employs a traditional salient-pole rotor with cage windings, known for its line-start capability, making it a feasible choice for constant-speed and pump applications. The proposed IPMSM, if viable, is expected to replace popular induction motors used in oil and gas pump stations and also for deep drilling, since IPMSMs are more efficient and easier to control [2] – [4].

## 2. Methodology

The proposed line-start, three-phase IPMSM consists of a conventional 36-slot distributed stator winding and a 4-pole dumbbell rotor with damper windings to dampen low-frequency oscillations. The parameters and dimensions of the proposed machine were derived from the conventional distributed SynRM and IPMSM [17], [18], and are presented in Table 1, with the inclusion of neodymium-iron-boron magnets placed inside the dumbbell rotor. Figure 1 shows the interior permanent magnet, the stator windings, and the rotor damper windings of the IPMSM.

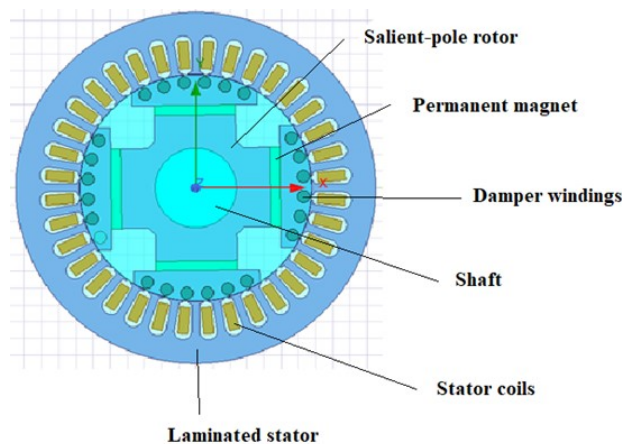


Figure 1. Stator winding and rotor of the IPMSM

Table 1. The machine circuit parameters and dimensions

Parameter	Value	Machine dimensions	Value
Frequency, F	50 Hz	Stator outer radius	105.2mm
Moment of inertia, J	0.0412 kg/m <sup>2</sup>	Stator inner radius	67.99mm
Permanent magnet flux linkage	0.4 Wb turn	Rotor radius	67.69mm
Rated power, P <sub>rated</sub>	5.5 kW	Effective stack length	160.22mm
Rated Speed	1500 rpm	Airgap length at pole face, g <sub>1</sub>	0.4mm
Rated Torque, T <sub>rated</sub>	35 Nm	Airgap length between poles, g <sub>2</sub>	21.3mm
Phase Voltage, V <sub>ph</sub>	370V	Stator slot depth	18mm
Stator resistance, R <sub>s</sub>	1.504 Ω	Ratio of pole arc to pole pitch	2/3
Stator leakage inductance, L <sub>ls</sub>	0.453 mH	Number of Pole pairs	2
Rotor d-axis leakage inductance, L <sub>ldr</sub>	2.5 mH	Number of winding layers	1
Rotor q-axis leakage inductance, L <sub>lqr</sub>	3.2 mH	Number of slots	36
Rotor d-axis resistance, R <sub>dr</sub>	0.12 Ω	Number of turns	32
Rotor q-axis resistance, R <sub>qr</sub>	0.25 Ω	Winding connection	Y

## 2.1. Voltage equations in direct-phase variables (Direct Phase Variable Model)

The voltage equation for IPMSM can be written as the synchronous machine equations without the damper winding and constant field dynamics. Therefore, the voltages in the stator reference frame can be expressed regarding instantaneous currents and flux linkages as follows;

$$V_{abc s} = r_{abc s} \cdot i_{abc s} + p \lambda_{abc s} \quad (1)$$

$$V_{qd r} = r_{qd r} i_{qd r} + \frac{d}{dt} \lambda_{qd r} \quad (2)$$

where,

$$\begin{cases} V_{abc s} = [V_{as} V_{bs} V_{cs}]^T \\ i_{abc s} = [i_{as} i_{bs} i_{cs}]^T \\ \lambda_{abc s} = [\lambda_{as} \lambda_{bs} \lambda_{cs}]^T \\ r_{abc s} = \text{diag}[R_s R_s R_s] \end{cases} \quad (3)$$

The “s” subscript denotes variables and parameters associated with the stator variables. The operator “p” represents the differentiating operation d/dt. For a magnetic linear system, the flux linkages can be calculated as presented in [19].

$$\lambda_{abcs} = L_{abcs} \cdot i_{abcs} + \lambda_{abcm} \quad (4)$$

where,

$$L_{abcs} = \begin{bmatrix} L_{aa}L_{ab}L_{ac} \\ L_{ba}L_{bb}L_{bc} \\ L_{ca}L_{cb}L_{cc} \end{bmatrix} \quad (5)$$

$$\lambda_{abcm} = \lambda_m \begin{bmatrix} \sin \theta_r \\ \sin(\theta_r - \frac{2\pi}{3}) \\ \sin(\theta_r + \frac{2\pi}{3}) \end{bmatrix} \quad (6)$$

The stator self and mutual inductances are expressed in equations (7) and (8), respectively.

$$\begin{cases} L_{aa} = L_{ls} + L_0 - L_{ms} \cos 2\theta_r \\ L_{bb} = L_{ls} + L_0 - L_{ms} \cos 2(\theta_r - \frac{2\pi}{3}) \\ L_{cc} = L_{ls} + L_0 - L_{ms} \cos 2(\theta_r + \frac{2\pi}{3}) \end{cases} \quad (7)$$

$$\begin{cases} L_{ab} = L_{ba} = -\frac{1}{2}L_0 - L_{ms} \cos 2(\theta_r - \frac{2\pi}{3}) \\ L_{ac} = L_{ca} = -\frac{1}{2}L_0 - L_{ms} \cos 2(\theta_r + \frac{2\pi}{3}) \\ L_{bc} = L_{cb} = -\frac{1}{2}L_0 - L_{ms} \cos 2(\theta_r + \pi) \end{cases} \quad (8)$$

In the above equations,  $L_{ls}$  is the stator leakage inductance,  $L_0$  and  $L_{ms}$  are the magnetising inductance components of the stator windings,  $\lambda_m$  is the flux linkage established by the rotor magnets.

The leakage inductance is the inductance that does not contribute to the transfer of power through the air gap. It should be noted that the magnetising inductance components are functions of the rotor position, and the coefficient  $L_{ms}$  is negative, while  $L_0$  is positive in the case of IPMSMs due to their unique rotor structure. Therefore, the quadrature-axis magnetising inductance  $L_{mq}$  is larger than the direct-axis magnetising inductance  $L_{md}$  of IPMSM, which is opposite to general salient-pole synchronous machines. The flux linkage equation in (4) can be extended to the form of

$$\begin{bmatrix} \lambda_{as} \\ \lambda_{bs} \\ \lambda_{cs} \end{bmatrix} = \begin{bmatrix} L_{aa}L_{ab}L_{ac} \\ L_{ba}L_{bb}L_{bc} \\ L_{ca}L_{cb}L_{cc} \end{bmatrix} \begin{bmatrix} i_{as} \\ i_{bs} \\ i_{cs} \end{bmatrix} + \lambda_m \begin{bmatrix} \sin \theta_r \\ \sin(\theta_r - \frac{2\pi}{3}) \\ \sin(\theta_r + \frac{2\pi}{3}) \end{bmatrix} \quad (9)$$

The inductances are a function of the rotor position  $\theta_r$  and therefore a function of the rotor speed  $\omega_r$ .

$$\theta_r = \int \omega_r dt \quad (10)$$

The mutual inductances between the stator windings and the rotor cage winding in the q-axis and d-axis are stated as

$$L_{asqr} = \sum_{k=1,3,5,\dots}^{\infty} L_{mq} \cos(p_r k \theta_r) \quad (11)$$

$$L_{asdr} = \sum_{k=1,3,5,\dots}^{\infty} L_{md} \sin(p_r k \theta_r) \quad (12)$$

where,

$$L_{mq} = \frac{3}{2} (L_0 - L_{ms}) \quad (13)$$

$$L_{md} = \frac{3}{2} (L_0 + L_{ms}) \quad (14)$$

where  $L_{md}$  and  $L_{mq}$  are the fictitious d-q axis magnetizing inductances, and  $k$  is the harmonic order.

Flux linkage can be stated in terms of rotor variables to stator windings as presented in (15).

$$\begin{bmatrix} \lambda_{abc} \\ \lambda'_{qdr} \end{bmatrix} = \begin{bmatrix} L_{abc} & L'_{abcqdr} \\ (L'_{abcqdr})^T & L'_{qdr} \end{bmatrix} \begin{bmatrix} i_{abc} \\ i'_{qdr} \end{bmatrix} \quad (15)$$

Therefore, inductance referred to the rotor parameter is given in (16) as:

$$L(\theta_r) = \begin{bmatrix} L_{abc} & L'_{abcqdr} \\ \frac{2}{3} (L'_{abcqdr})^T & L'_{qdr} \end{bmatrix} \quad (16)$$

Referring the self-inductances of the rotor cage windings to the stator will give equation (17),

$$L'_{qdr} = \begin{bmatrix} L'_{lqr} + L_{mq} & 0 \\ 0 & L'_{ldr} + L_{md} \end{bmatrix} \quad (17)$$

The electromagnetic torque of the proposed IPMSM is presented in (18)

$$T_{em} = \frac{p}{2} \left\{ \begin{aligned} & i_{abc}^T \frac{\partial L_{abc}}{\partial \theta_r} i_{abc} + i_{abc}^T \frac{\partial L_{abcqdr}}{\partial \theta_r} i_{qdr} \\ & + \frac{\partial L_{abcqdr}^T}{\partial \theta_r} i_{abc} + i_{qdr}^T \frac{\partial L_{qdr}}{\partial \theta_r} i_{qdr} \end{aligned} \right\} \quad (18)$$

The relationship between the electromagnetic torque of the machine ( $T_{em}$ ) and rotor speed ( $\omega_r$ ) is given in the mechanical dynamic equation while ignoring the effect of friction:

$$T_g = J \left( \frac{2}{p} \right) p_r \omega_r + B_m \left( \frac{2}{p} \right) \omega_r + T_L \quad (19)$$

where  $J$  is the total inertia of the rotating mass,  $T_L$  is the load torque, and  $p_r$  is the number of rotor pole pairs. The constant  $B_m$  is a damping coefficient that is generally small and often neglected.

## 2.2. Dynamic simulation of the IPMSM

The dynamic simulation of the three-phase line-start IPMSM was realized using MATLAB/Simulink. The simulation was done in direct-phase variables (DPV) using only the fundamental harmonic. The motor's circuit specifications and machine dimensions used for the simulation are presented in Table 1. The magnetizing d-q inductances of the motor windings used for the simulation were calculated as  $L_{mq} = 7.88$  mH and  $L_{md} = 2.99$  mH. The procedure used for the calculation was similar to what was presented in [20]. The line-start IPMSM's initial transient and dynamic behaviour were observed. At 1 second, a load torque of 25 Nm, about (70% of rated torque) was applied to evaluate the dynamic behaviour of the DPV model.

## 2.3. Finite element analysis of the IPMSM

The finite element method (FEM) is a numerical technique that breaks a large problem space down into smaller spaces, known as finite elements, through the use of meshes. The FEA mesh plot is shown in Figure 2. Using FEA in the analysis of electrical machines, the electric and magnetic fields of the machines are determined [21].

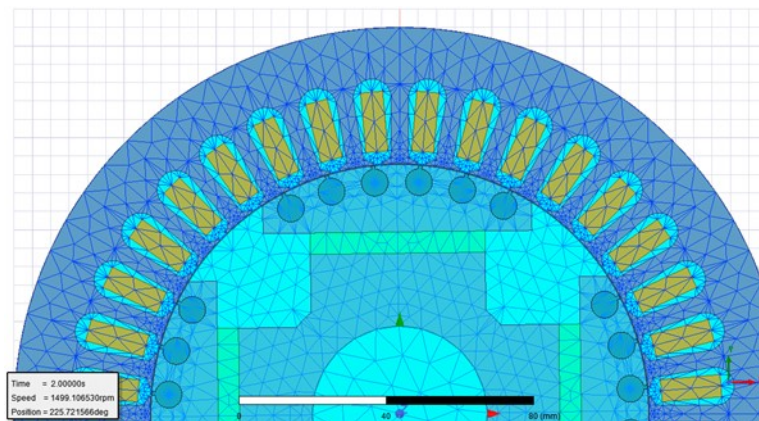


Figure 2. FEA Mesh plot of the IPMSM

The dynamic simulation of the proposed IPMSM was carried out in Ansys Maxwell Electronics Desktop FEA software for validation. The design parameters given in Table 1 for validation of the motor model were used for this analysis. The IPMSM was also simulated as a line-start with a supply voltage of 370 V at a frequency of 50 Hz. A simulation time of 2 seconds was used, and a 25 Nm load torque was introduced after 1 second. The speed, torque, phase currents, self and inductances, and torque-speed performance characteristics of the machine were then observed and presented alongside the results obtained from the DPV model.

## 3. Results and discussion

The performance characteristics of the IPMSM in direct-phase variables and FEA are presented in this section. In Figure 3, the speed characteristics of the DPV model and FEA were presented. According to the DPV model speed plot in Figure 4, the IPMSM took roughly 0.25 seconds to reach a

synchronous speed of 1500 rpm following an initial speed transient surge of 1844 rpm at start-up. A transient speed rise of 1544 rpm was recorded for the FEA model at start-up after 1 second, which later settled at a synchronous speed of 1501 rpm at 0.08 seconds.

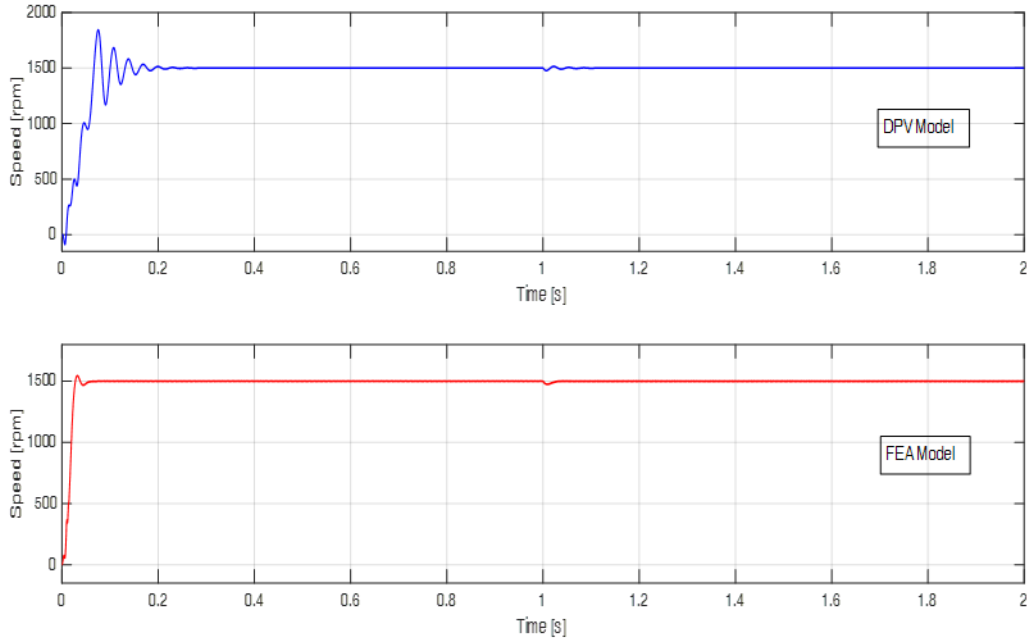


Figure 3. IPMSM rotor speed

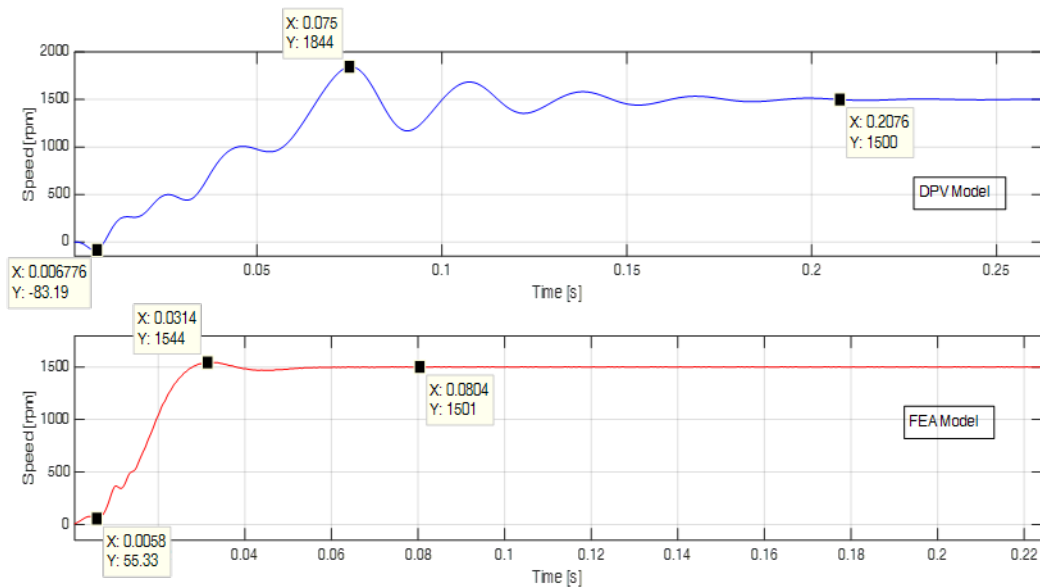


Figure 4. IPMSM speed transient at start-up

The results show minor deviations from synchronism that is damped after a short amount of time due to the damper windings on the rotor, as seen in Figure 4. The torque characteristic of the DPV model shown in Figures 5 - 7 exhibited slight evidence of torque pulsations induced by MMF of the concentrated non-overlapping winding stator. At start-up, an initial torque rise of 179.5 Nm settled with ripples at about 0.3 seconds. The torque ripple plot in Figure 6 was extrapolated from the torque

performance plots in Figure 5. In Figure 6, the extrapolation was done before the introduction of load torque. The maximum and minimum torque ripple values are seen on the extrapolated plots. Figure 7 presents the torque ripple values at the introduction of load.

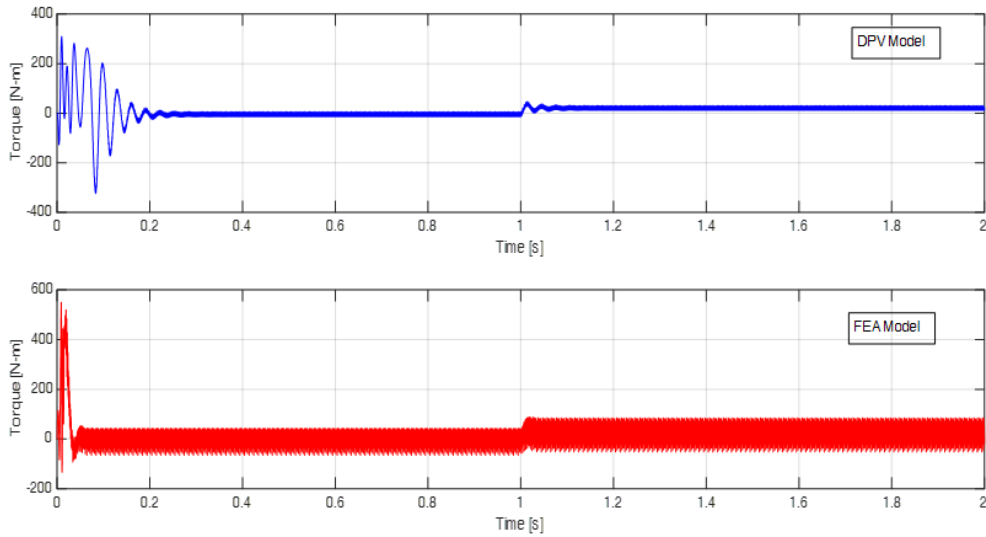


Figure 5. IPMSM torque against time

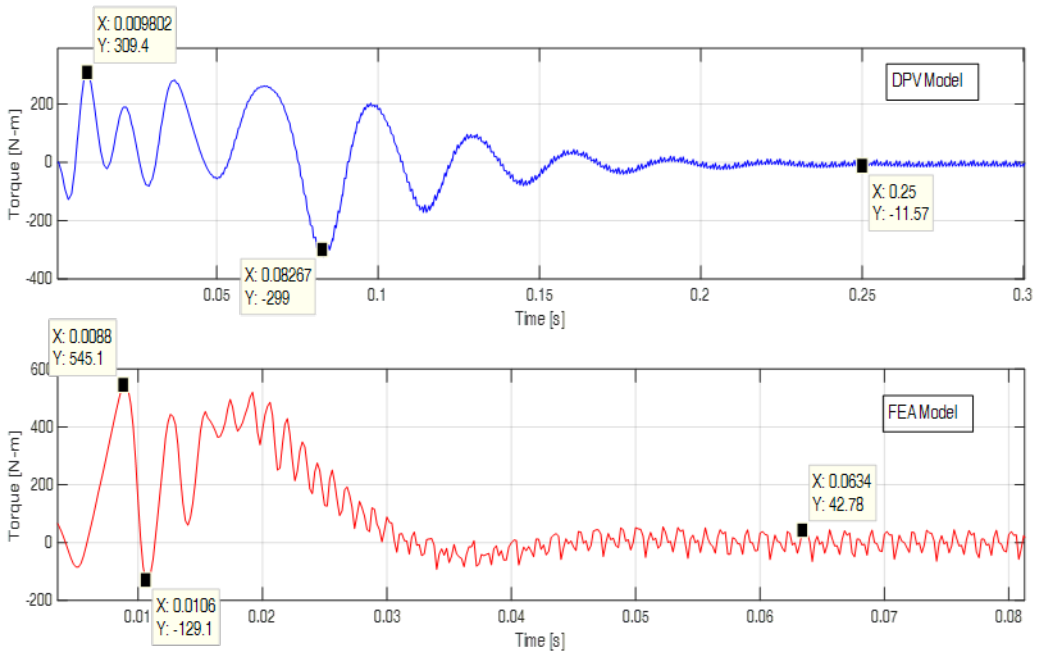


Figure 6. IPMSM torque transient at start-up

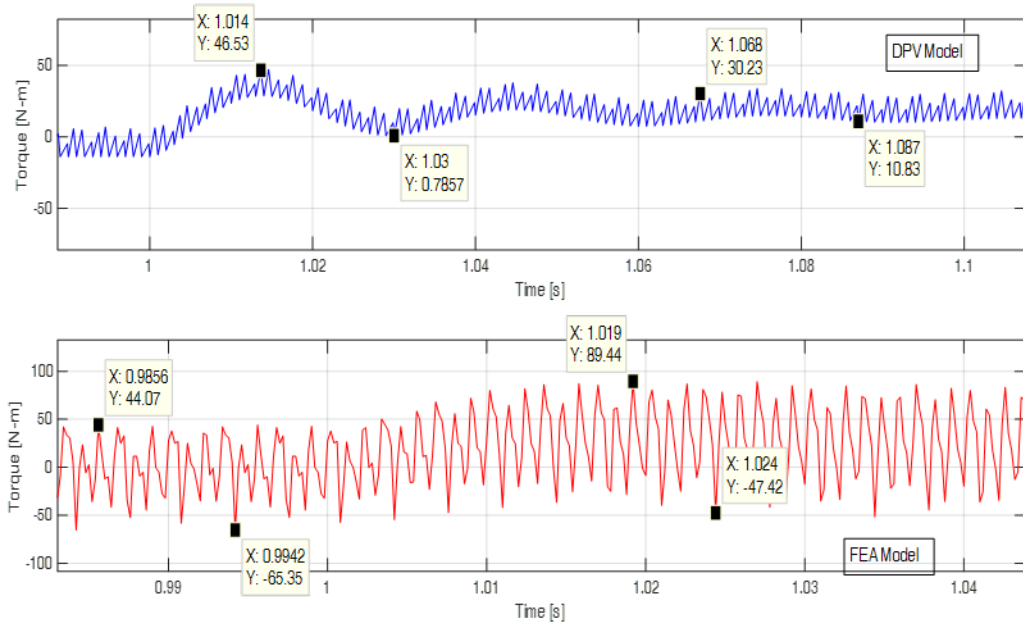


Figure 7. IPMSM torque ripples at the introduction of load

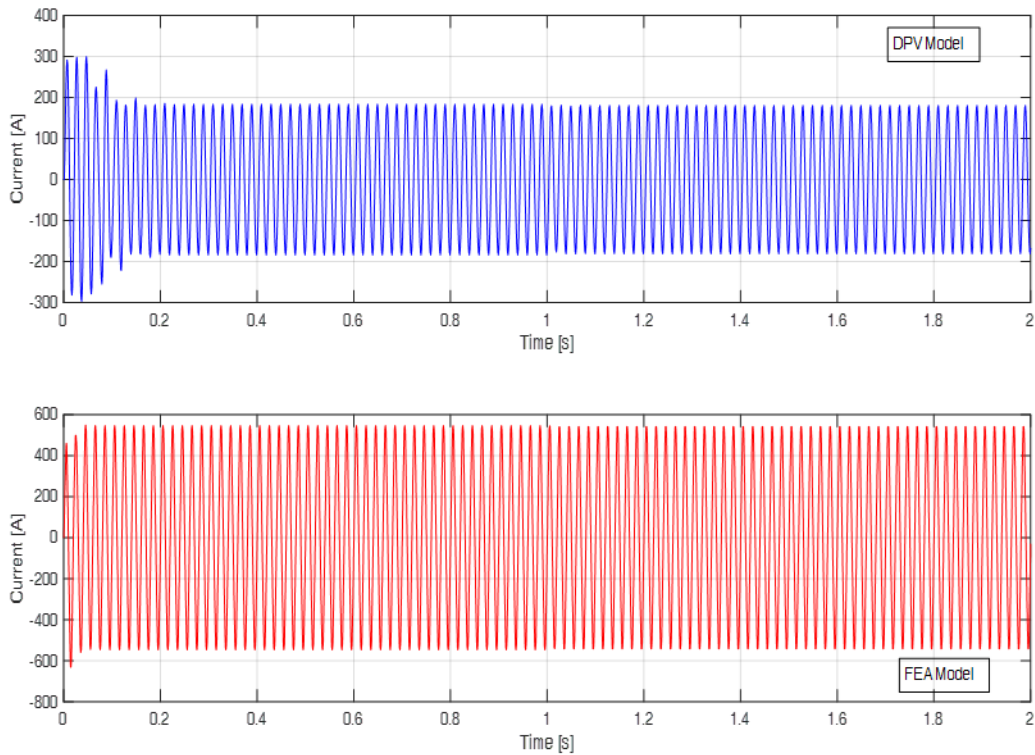


Figure 8. IPMSM stator phase current

The Stator phase A currents of both DPV and FEA models are presented in Figure 8. The NVM current plot shows the stator winding phase A current, similar to the currents obtained in phases B and C, with a starting transient current of 300 A and later settling at 190 A. The stator phase current of the FEA plot was observed as 371 A (RMS). Both plots were quite similar and in good agreement. The torque-speed characteristics represent the correlation between the speed and torque of the machine during the operation phases, from start to full load speed. In Figure 9, the torque-speed plots revealed that an initial settling torque value of 0 Nm was attained at synchronous speed. When a load was applied, the torque value rose from 0 Nm to a settling value of 25 Nm, indicating full load torque at full load speed. The effects of MMF harmonics were very visible in the torque-speed plot of the FEA model, which was not seen in the DPV model.

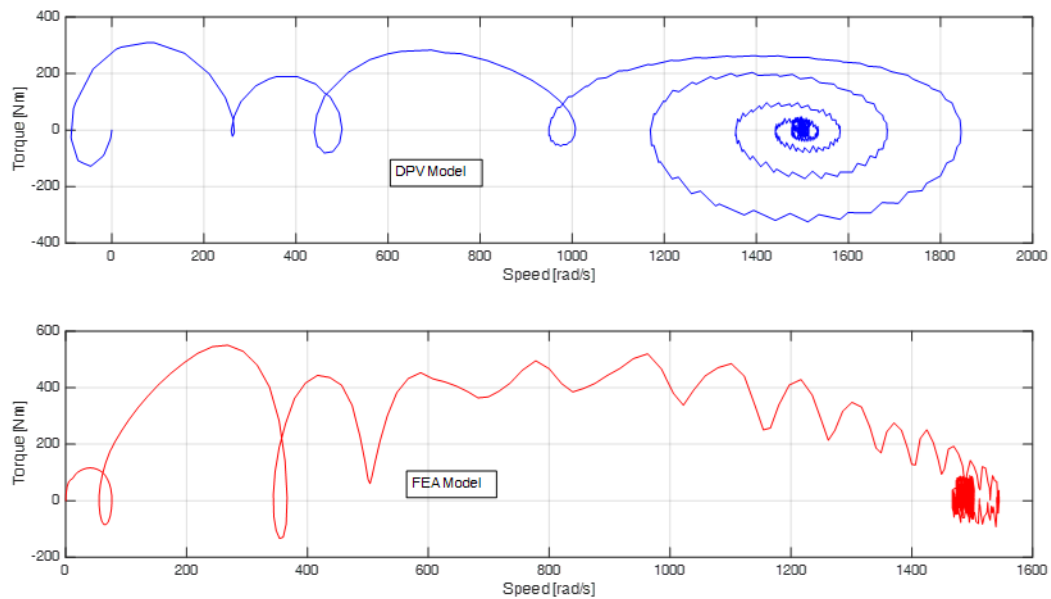


Figure 9. IPMSM torque-speed characteristic

The field plots of the IPMSM are presented in Figures 10 and 11. At a rotor position of 225.72°, the magnetic flux density of the model presented in Figure 10 had a maximum magnetic flux density of 2.716T. The magnetic vector potential in Figure 11 was 0.0414 Wb/m at its maximum and -0.0414 Wb/m at its minimum.

Maxwell's equations derived the field plots in ANSYS [22]. The plot is not possible in MATLAB/Simulink using the DPV method. The magnetic flux densities and magnetic flux line distributions of the IPMSM are visible in the plots. The field plot revealed increased magnetic flux density and flux distribution on the motor's stator laminations as well as on the rotor pole face between the cage windings.

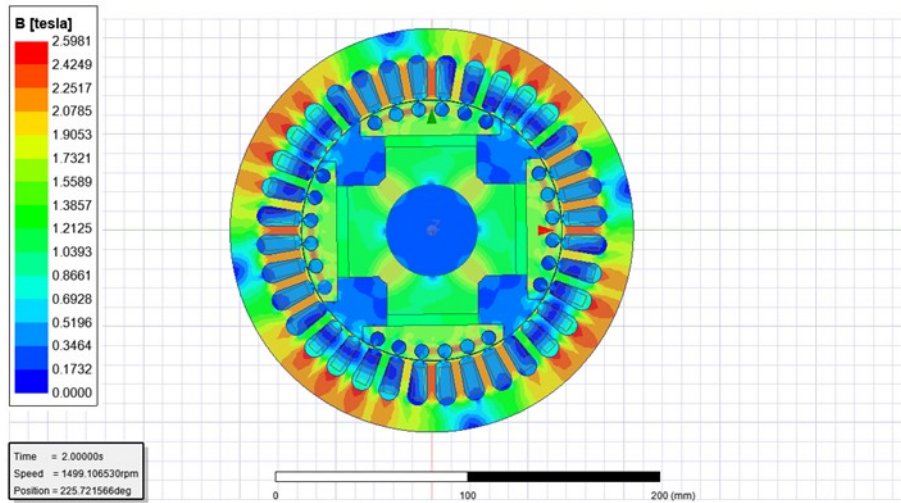


Figure 10. IPMSM FEA magnetic flux density

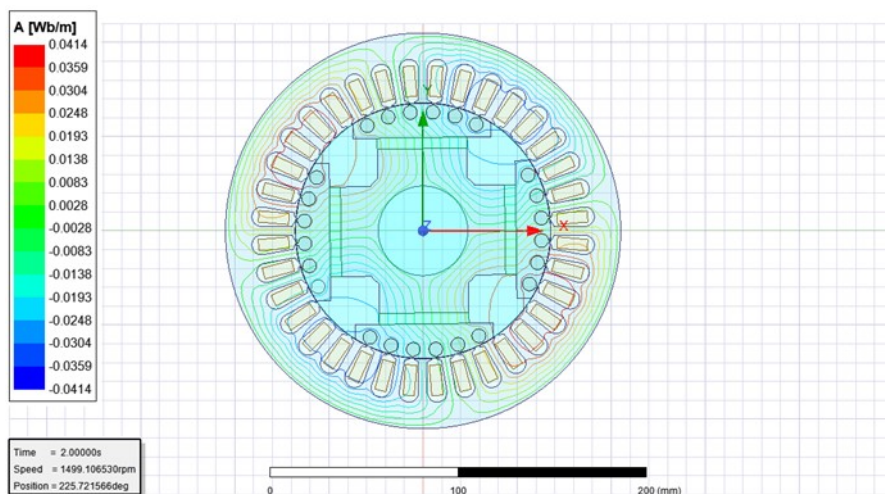


Figure 11. IPMSM FEA magnetic vector potential showing flux lines

#### 4. Conclusion

The direct phase variable (DPV) model was used to simulate the proposed IPMSM and was validated using finite element analysis (FEA). In the DPV and FEA models, the proposed IPMSM was simulated as a line-start with a three-phase voltage supply of 370 V. The FEA torque plots revealed more torque ripple caused by the MMF harmonics of the stator winding and the rotor design, which would not be visible in the DPV model. Although the FEA model validated that the IPMSM is implementable and also showed evidence of MMF harmonics in its results, meaning it is more accurate, it does not invalidate the results from the DPV model as both results are in good agreement.

The IPMSM with a traditional salient-pole rotor with cage windings has an advantage over other rotor types due to its line-start capability. Hence, the proposed motor is feasible and can be used

in constant-speed applications and also for pump applications in the oil and gas industry. The DPV model can also be used in other AC machine analyses because it provides some form and accuracy without requiring complex transformations, as seen in the popular conventional d-q model.

## Conflict of interest

The authors have no competing interests to declare that are relevant to the content of this article.

## References

- [1] Dulanto, A. O. (2015). Design of a synchronous reluctance motor assisted with permanent magnets for pump applications. (Doctoral dissertation). *KTH Royal Institute of Technology, Stockholm*.
- [2] Lutfrakhmanovich, G. A., Dinarovich, K. R., Rustemovich, U. R., & Igorevich, S. D. (2019, October). Features of the permanent magnet submersible electric motors design for the oil industry. In *2019 International Conference on Electrotechnical Complexes and Systems (ICOECS)*. 1-5. <https://doi.org/10.1109/ICOECS46375.2019.8950019>.
- [3] Cui, J., Xiao, W., Zhang, X., Zhang, X., Zhang, P., Chen, P., Huang, H., & Wu, X. (2016, November). Electric submersible progressing cavity pump driven by low-speed permanent magnet synchronous motor. In *SPE Middle East Artificial Lift Conference and Exhibition*. 1-11. <https://doi.org/10.2118/184228-MS>
- [4] Bafghi, M. B., & Vahedi, A. (2018, November). A comparison of electric motors for electrical submersible pumps used in the oil and gas industry. In *IOP Conference Series: Materials Science and Engineering*, 433(1), 1-12. <https://doi.org/10.1088/1757-899X/433/1/012091>
- [5] Umoh, G., Ogbuka, C., & Obe, E. S. (2020). Modelling and analysis of five-phase permanent magnet synchronous motor in machine variables. *Przegląd Elektrotechniczny*, 96(1), 87-92. <https://doi.org/10.15199/48.2020.01.21>.
- [6] Tola, O. J., Obe, E. S., & Anih, L. U. (2017, November). Modeling and analysis of dual stator windings permanent magnet synchronous motor. In *2017 IEEE 3rd International Conference on Electro-Technology for National Development (NIGERCON)*, 861-871. <https://doi.org/10.1109/NIGERCON.2017.8281954>
- [7] Cho, S. K., Jung, K. H., & Choi, J. Y. (2018). Design optimization of interior permanent magnet synchronous motor for electric compressors of air-conditioning systems mounted on EVs and HEVs. *IEEE Transactions on Magnetics*, 54(11), 1-5. <https://doi.org/10.1109/TMAG.2018.2849078>
- [8] Chen, H., & Lee, C. H. (2019). Parametric sensitivity analysis and design optimization of an interior permanent magnet synchronous motor. *IEEE Access*, 7, 159918-159929. <https://doi.org/10.1109/ACCESS.2019.2950773>
- [9] Toliyat, H. A., Rahimian, M. M., & Lipo, T. A. (1991, October). dq modeling of five phase synchronous reluctance machines including third harmonic of air-gap MMF. In *Conference Record of the 1991 IEEE Industry Applications Society Annual Meeting*, 231-237. <https://doi.org/10.1109/IAS.1991.178160>
- [10] Peng, W., Gyselinck, J., Dziechciarz, A., & Martis, C. (2016, April). Magnetic equivalent circuit modelling of Reluctance Machines. In *2016 Eleventh International Conference on Ecological Vehicles and Renewable Energies (EVER)*, 1-7. <https://doi.org/10.1109/EVER.2016.7476429>
- [11] Obe, E. S., & Binder, A. (2011). Direct-phase-variable model of a synchronous reluctance motor including all slot and winding harmonics. *Energy conversion and management*, 52(1), 284-291. <https://doi.org/10.1016/j.enconman.2010.06.069>
- [12] Umoh, G., Obe, C., Ogbuka, C., Ekpo, G., & Obe, E. (2020). Direct-phase variable modelling and analysis of five-phase synchronous reluctance motor for direct-on-line starting. *Przegląd Elektrotechniczny*, 97(1), 24-29. <https://doi.org/10.15199/48.2021.01.05>

- [13] Epemu, A., Obe, P., & Obe, E. (2021). Modelling and analysis of concentrated and distributed winding synchronous reluctance motors in direct-phase variables and finite element analysis. *Przełąd Elektrotechniczny*, 97. <http://dx.doi.org/10.15199/48.2021.10.14>
- [14] Epemu, A. M., & Obe E. S. (2021, May) "Performance Evaluation of Synchronous Reluctance Motors with different Concentrated Stator Winding Topologies," in *Proceedings of the 2nd International Conference on Electrical Power Engineering (ICEPENG 2021)*. 5–10. [https://drive.google.com/file/d/1mmJCOTQvday4cqI\\_JQ95965nxWxoUXjN/view](https://drive.google.com/file/d/1mmJCOTQvday4cqI_JQ95965nxWxoUXjN/view)
- [15] Vu Xuan, H. (2012). Modeling of exterior rotor permanent magnet machines with concentrated windings. <http://resolver.tudelft.nl/uuid:27bb59c4-14c8-45fe-9284-28363b46e060>
- [16] Karimagako, R., Nagrial, M. H., & Rizk, J. (2010, April). Analysis and design of permanent magnet assisted synchronous reluctance machines. In *5th IET International Conference on Power Electronics, Machines and Drives (PEMD 2010)*, 1-6. <https://doi.org/10.1049/cp.2010.017>
- [17] Obe, E. S. (2009). Direct computation of ac machine inductances based on winding function theory. *Energy Conversion and Management*, 50(3), 539-542. <https://doi.org/10.1016/j.enconman.2008.10.017>
- [18] Ong, C. M. (1998) *Dynamic Simulation of Electrical machinery, Using Matlab/Simulink*," Prentice Hall, Upper Saddle River.
- [19] Krause, P. C., Wasynczuk, O., Sudhoff, S. D., & Pekarek, S. D. (2013). *Analysis of electric machinery and drive systems* (Vol. 75). John Wiley & Sons. Hoboken. New Jersey.
- [20] Obe, E. S. (2010). Calculation of inductances and torque of an axially laminated synchronous reluctance motor. *IET electric power applications*, 4(9), 783-792. <https://doi.org/10.1049/iet-epa.2009.0197>
- [21] Bianchi, N. (2017). *Electrical machine analysis using finite elements*. CRC press. Boca Raton. <https://doi.org/10.1201/9781315219295>